Dielectric response of doped organic semiconductor devices: P3HT:PCBM solar cells

Oskar Armbruster,[1,*] Christoph Lungenschmied,[2,†] and Siegfried Bauer[1]
[1]*Department of Soft Matter Physics, Johannes Kepler University, Altenberger Straße 69, A-4040 Linz, Austria*
[2]*Konarka Austria F&E GmbH, Altenberger Straße 69, A-4040 Linz, Austria*
(Received 6 March 2011; published 26 August 2011)

We introduce a model to account for the dielectric response of doped organic semiconductor devices. In addition to the phenomena observed for undoped devices, mobile charge carriers created by doping can alter the dielectric function of the organic material and hence the dielectric response of the devices. These extrinsic charges may be trapped and contribute to the capacitance on re-emission. We directly model the real part of the dielectric function based on this phenomenon. The imaginary part is obtained via the application of the Kramers-Kronig transformation. We use oxygen-doped poly(3-hexylthiophene):[6,6]-phenyl-C_{61}-butyric acid methyl ester– (P3HT:PCBM) based organic solar cells as a model system to test our approach and hence contribute to the understanding of oxygen-induced degradation in these devices. We fit our equations to the measured dielectric data and compare it to Debye relaxation as well as two widely used equivalent circuit models. Together with the device resistance determined from the steady-state current-voltage characteristic around 0V an excellent agreement between the experimental data and our model is achieved for both the real and the imaginary part of the dielectric function over a frequency range covering five orders of magnitude. Unlike the Debye relaxation model or the equivalent circuit approach, our model yields important device parameters such as the dopant concentration.

DOI: 10.1103/PhysRevB.84.085208 PACS number(s): 88.40.jr, 77.22.Gm, 73.50.Gr, 68.55.Ln

I. INTRODUCTION

The sun emits approximately 175 PW into the solid angle covered by the Earth. Hence, the energy delivered to the Earth within 45 min exceeds the primary energy requirement of humankind in 2009 of approximately 467 EJ.[1] Harvesting solar energy promises to significantly reduce the emission of CO_2 and thus provides a firm base for a sustainable energy market. Although the supply of solar irradiation is plentiful, only a marginal part is currently converted into electrical energy. The cumulative solar cell production until 2010 is reported to be 31 GWp.[2] Unlike most established photovoltaic technologies based on inorganic semiconductors, organic bulk-heterojunction solar cells can be processed from inks by using industrial-scale printing processes. This technology offers the possibility for large-scale production to meet the needs of a growing energy demand. Conjugated polymer/fullerene-based organic photovoltaic (OPV) devices have reached efficiencies of up to 8.3%, confirmed by accredited certification labs.[3,4] As first products incorporating polymer-based OPV are available on the market, module stability and lifetime become key parameters of concern.[5] Various processes have been reported to contribute to the degradation of OPV devices; however, oxygen and water are frequently named to be most dominating.[5–7] A detailed understanding of the degradation processes in OPV devices may help to improve module lifetimes and hence increase market opportunities.

We herein present a general model to describe impedance spectra of doped organic semiconductor devices by using the example of organic solar cells exposed to oxygen. Dielectric spectroscopy is a widely used technique in the field of organic semiconductor research. It has been applied to gain insight into many fundamental processes taking place in these devices, including charge carrier transport and recombination. A good understanding of the impedance features of poly (*p*-phenylene vinylene)- (PPV) based devices without applied bias as well as for predominant hole current was established by Martens *et al*.[8] However, the dielectric response of undoped PPV-based devices and significantly doped organic semiconductors was found to differ fundamentally. Scherbel *et al*. studied devices based on PPV prepared by the so-called precursor route,[9] which showed a significant concentration of extrinsic charge carriers. In order to model the broadband dielectric response they constructed equivalent circuits with multiple elements, each one consisting of a capacitor and a resistor connected in parallel. Boix *et al*. chose a different way to describe impedance data measured on organic semiconductor devices. They derived a model analyzing the dielectric response in terms of the energy distribution of defect states.[10] The formalism describes the organic semiconductor as a dielectric with a frequency-independent relative permittivity in which charge carriers with a frequency-dependent response are embedded. Assuming that the relative permittivity of the material in which the charge carriers are embedded is independent of frequency conflicts with the results of Martens *et al*. described above.[8]

In Sec. II the established approaches such as Debye relaxation and the impedance response of two equivalent circuits that are commonly used to assess dielectric data of doped organic semiconductor devices are outlined. These models serve as a basis for comparing our approach of describing the dielectric response. We then introduce a formalism describing the dielectric permittivity of doped organic semiconductor devices at zero dc bias. It includes the influence of the frequency on the ability of charge carriers to respond to an externally applied ac signal. In addition, we apply the approach of Martens *et al*. of a frequency-dependent dispersive permittivity. The sum of these two contributions yields an explicit description for the real part of the dielectric function. The imaginary part cannot be directly derived with

our approach. However, the imaginary part is obtained by performing the Kramers-Kronig transformation. In Sec. III the measurement details are described. We test our model on experimental results obtained from oxygen doped, state of the art, semitransparent poly(3-hexylthiophene):[6,6]-phenyl-C_{61}-butyric acid methyl ester– (P3HT:PCBM) based organic solar cells and compare it to the above-mentioned established ways of interpreting the dielectric response of doped organic semiconductors (Sec. IV).

II. MODELS

A. Debye relaxation

Debye relaxation describes the response of ideal, noninteracting dipoles to the applied ac field. The complex permittivity ε_D is given by

$$\varepsilon_D = \frac{\Delta\varepsilon}{1+\hat{\imath}\omega\tau} + \varepsilon_\infty,$$

where ε_∞ and $\Delta\varepsilon + \varepsilon_\infty$ are the high- and low-frequency limit of relative permittivity and τ is the characteristic relaxation time of the medium.[11]

Separating $\underline{\varepsilon}_D$ in real part ε'_D and imaginary part ε''_D yields

$$\varepsilon'_D = \frac{\Delta\varepsilon}{1+\omega^2\tau^2} + \varepsilon_\infty, \tag{1}$$

$$\varepsilon''_D = \frac{\Delta\varepsilon}{1+\omega^2\tau^2}\tau\omega. \tag{2}$$

In this representation, ε'_D describes the frequency-dependent storage, whereas ε''_D accounts for the frequency-dependent dielectric loss resulting from the frequency dependence of ε'_D. For fitting experimental data, a second contribution to the imaginary part of relative permittivity resulting from the finite dc resistance of the dielectric has to be considered. Formally speaking, a parallel-plate capacitor of surface area A and plate separation d that is filled with a Debye-dielectric is connected in parallel to an ohmic resistor R. This causes an additive contribution to imaginary part of the relative permittivity of

$$\varepsilon_R = \hat{\imath}\frac{d}{A\varepsilon_0\omega}R^{-1} \tag{3}$$

resulting in

$$\varepsilon''_{D+R} = \frac{\Delta\varepsilon}{1+\omega^2\tau^2}\tau\omega + \frac{d}{A\varepsilon_0\omega}R^{-1}.$$

B. Equivalent circuits

Equivalent circuit models are widely used to describe the dielectric response of organic semiconductor devices.[9,12] Such equivalent circuits can be made arbitrarily complex and are a convenient way to model the dielectric response with only two physical concepts, namely ideal resistors and ideal capacitors.

Certain parts of the equivalent circuit are usually assigned to different regions in the device, such as bulk and depletion layer. Two frequently used equivalent circuits are shown in Fig. 1. The impedance Z of these two equivalent circuits is given by

$$Z_{RC,(a)} = \left\{R_1^{-1} + \left[(\hat{\imath}\omega C_1)^{-1} + \left(R_2^{-1} + \hat{\imath}\omega C_2\right)^{-1}\right]^{-1}\right\}^{-1}$$

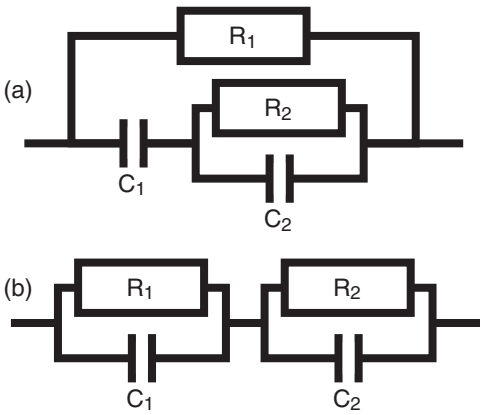

FIG. 1. Two equivalent circuits that are formally identical to Debye relaxation.

and

$$Z_{RC,(b)} = \left(R_1^{-1} + \hat{\imath}\omega C_1\right)^{-1} + \left(R_2^{-1} + \hat{\imath}\omega C_2\right)^{-1}.$$

Rewriting the complex impedance of the equivalent circuits in ε' and ε'' and appropriately grouping the terms reveals that these are formally identical to Debye relaxation, including the correction for the finite dc resistance:

$$\varepsilon'_{RC,(a)} = \frac{\overbrace{\frac{d}{A\varepsilon_0}\frac{C_1^2}{C_1+C_2}}^{\Delta\varepsilon}}{1+\omega^2\underbrace{[(C_1+C_2)R_2]^2}_{\tau^2}} + \underbrace{\frac{d}{A\varepsilon_0}\frac{C_1C_2}{C_1+C_2}}_{\varepsilon_\infty}$$

$$\varepsilon''_{RC,(a)} = \frac{\overbrace{\frac{d}{A\varepsilon_0}\frac{C_1^2}{C_1+C_2}}^{\Delta\varepsilon}}{1+\omega^2\underbrace{[(C_1+C_2)R_2]^2}_{\tau^2}} \times \underbrace{(C_1+C_2)R_2}_{\tau}\omega + \frac{d}{A\varepsilon_0\omega}\underbrace{R_1^{-1}}_{R^{-1}}$$

$$\varepsilon'_{RC,(b)} = \frac{\overbrace{\frac{d}{A\varepsilon_0}\frac{(C_1R_1-C_2R_2)^2}{(C_1+C_2)(R_1+R_2)^2}}^{\Delta\varepsilon}}{1+\omega^2\underbrace{(C_1+C_2)^2\frac{R_1^2R_2^2}{(R_1+R_2)^2}}_{\tau^2}} + \underbrace{\frac{d}{A\varepsilon_0}\frac{C_1C_2}{C_1+C_2}}_{\varepsilon_\infty}$$

$$\varepsilon''_{RC,(b)} = \frac{\overbrace{\frac{d}{A\varepsilon_0}\frac{(C_1R_1-C_2R_2)^2}{(C_1+C_2)(R_1+R_2)^2}}^{\Delta\varepsilon}}{1+\omega^2\underbrace{(C_1+C_2)^2\frac{R_1^2R_2^2}{(R_1+R_2)^2}}_{\tau^2}} \times \underbrace{(C_1+C_2)\frac{R_1R_2}{R_1+R_2}}_{\tau}\omega + \frac{d}{A\varepsilon_0\omega}\underbrace{(R_1+R_2)^{-1}}_{R^{-1}}.$$

Since Debye relaxation and the two above equivalent circuits are mathematically identical, it is thus possible to determine the parameters C_1, C_2, R_1, and R_2 from the Debye

parameters $\Delta\varepsilon$, ε_∞, τ, and R or vice versa. We will thus not treat the equivalent circuits further.

C. Density of states for charges

As a consequence of the doping process, mobile charges are present in the active layer of an organic semiconductor device.[7] Their ability to respond to an externally applied ac signal is limited by the presence of trap states that can capture the charge carrier, immobilize it for a certain period of time, and eventually release it again. The average trapping time depends on the depth and capture cross section of a trap and on the temperature of the charge carrier. Applying an ac voltage to the two electrodes causes a periodic displacement of the mobile charge carriers in the polymer. The frequency of the ac voltage determines the average distance a charge carrier can move in one half-cycle. This movement of a charge carrier through the material is determined by the buildup of the electric field inside the device. It thus contributes to the out-of-phase current response (i.e., the capacitance) and is eventually limited by traveling from one electrode to the other.

We describe our samples as a parallel-plate capacitor filled with a dielectric of relative permittivity ε_g. The geometric capacitance C_g is thus given by

$$C_g = \varepsilon_g \varepsilon_0 \frac{A}{d},$$

where ε_0 is the vacuum permittivity, A is the surface area of the electrodes, and d is the thickness of the dielectric.

Doping introduces additional charge carriers in the active layer that cause the low-frequency capacitance C to significantly exceed the geometric capacitance C_g. The amount of charges N is thus given by

$$N = \frac{(C - C_g)U_{\mathrm{bi}}}{q},$$

where U_{bi} is the built-in voltage caused by the asymmetry of the metal-semiconductor contacts and q is the elementary charge. In the presence of traps the charges may be immobilized for a certain time and contribute only to the capacitance when re-emitted. In order to account for this phenomenon, we introduce a density of trap states (DOS) g, conventionally defined as:

$$g = \frac{1}{V}\frac{dN}{dE},$$

where $V = Ad$ is the volume of the dielectric layer and E is the energy of the respective state.

We assume that the correlation between E and the frequency of the applied ac voltage f is given by a Boltzmann factor where ν is the attempt-to-escape (ATE) frequency that depends on the properties of the active layer.[10,13–17] T denotes the absolute temperature and k_B is the Boltzmann constant:

$$f(E) = \nu \exp\left[-\frac{E}{k_B T}\right]. \tag{4}$$

The DOS can now be rewritten in terms of parameters experimentally accessible via dielectric spectroscopy.

$$g = \frac{1}{V}\underbrace{\frac{dN}{d(C-C_g)}}_{\frac{U_{bi}}{q}}\frac{d(C-C_g)}{df}\underbrace{\frac{df}{dE}}_{-\frac{f}{k_B T}}$$
$$= -\frac{U_{\mathrm{bi}}}{qk_B TV} f \frac{d(C-C_g)}{df}. \tag{5}$$

We model the experimental DOS with a Gaussian curve located at the central energy E_0 and a width σ:[10,16,18,19]

$$g = \frac{N}{\sqrt{2\pi}\sigma}\exp\left[-\frac{(E_0 - E)^2}{2\sigma^2}\right].$$

In Eq. (4), E_0 and E can be substituted by using frequencies f_0 and f that are experimentally accessible, hence eliminating the dependence on the ATE frequency ν in this representation:

$$g = \frac{N}{\sqrt{2\pi}\sigma}\exp\left[-\frac{k_B^2 T^2}{2\sigma^2}\ln^2\frac{f}{f_0}\right]. \tag{6}$$

Combining Eq. (5) and Eq. (6) results in

$$dC = -\frac{qk_B TVN}{\sqrt{2\pi}\sigma U_{\mathrm{bi}}}\frac{1}{f}\exp\left[-\frac{k_B^2 T^2}{2\sigma^2}\ln^2\frac{f}{f_0}\right]df + dC_g.$$

Integration on both sides yields

$$C = \frac{qVN}{2U_{\mathrm{bi}}}\left(1 - \mathrm{erf}\left[\frac{k_B T}{\sqrt{2}\sigma}\ln\frac{f}{f_0}\right]\right) + C_g,$$

where erf is the Gaussian error function.

The real part of the relative permittivity is thus given by

$$\varepsilon'_{\mathrm{DOS}} = \frac{qd^2 N}{2\varepsilon_0 U_{\mathrm{bi}}}\left(1 - \mathrm{erf}\left[\frac{k_B T}{\sqrt{2}\sigma}\ln\frac{f}{f_0}\right]\right) + \varepsilon_g.$$

The DOS model does not yield an explicit expression for the imaginary part of the relative permittivity $\varepsilon''_{\mathrm{DOS}}$. Complex relative permittivity, however, needs to obey the Kramers-Kronig relation[20,21] given by

$$\varepsilon'(f) = \frac{1}{\pi}\mathcal{P}\int_{-\infty}^{+\infty} d\tilde{f}\,\frac{\varepsilon''(\tilde{f})}{\tilde{f} - f} \quad \text{and}$$
$$\varepsilon''(f) = -\frac{1}{\pi}\mathcal{P}\int_{-\infty}^{+\infty} d\tilde{f}\,\frac{\varepsilon'(\tilde{f})}{\tilde{f} - f}, \tag{7}$$

where $\mathcal{P}\int$ is the Cauchy principal value integral.

By using Eq. (7) $\varepsilon''_{\mathrm{DOS}}$ can be calculated from $\varepsilon'_{\mathrm{DOS}}$.

1. Static DOS model

In the derivation above, only the contribution of extrinsic charges is modeled. In order to include the background response of the undoped semiconductor, the simplest approach is to assume a frequency-independent relative permittivity of $\varepsilon_{g,s}$. Such a static DOS model formalism is given by

$$\varepsilon'_{\mathrm{DOS},s} = \frac{qd^2 N}{2\varepsilon_0 U_{\mathrm{bi}}}\left(1 - \mathrm{erf}\left[\frac{k_B T}{\sqrt{2}\sigma}\ln\frac{f}{f_0}\right]\right) + \varepsilon_{g,s}. \tag{8}$$

2. *Dispersive DOS model*

Martens *et al.* presented a model that describes the complex admittance response of PPV.[8] They observed a broad dispersion in case of zero bias. Equation (8), however, assumes a frequency-independent response (the geometric capacitance ε_g). We hence utilize their model to describe the frequency dependence of the contribution of the undoped semiconductor by replacing the constant ε_g in Eq. (8) by a dispersive term. The real part of the model of Martens *et al.* represented as relative permittivity is given by

$$\varepsilon_{g,d} = \frac{\varepsilon_{\infty,d}}{2}\frac{\omega^2 h}{g^2+h^2}$$

with

$$p = 2M\omega^\gamma \sin\frac{\pi\gamma}{2} + M^2\omega^{2\gamma}\sin(\pi\gamma),$$
$$q = 1 + 2M\omega^\gamma \cos\frac{\pi\gamma}{2} + M^2\omega^{2\gamma}\cos(\pi\gamma),$$
$$r = \left(1 + M\omega^\gamma \cos\frac{\pi\gamma}{2}\right)^2 + M^2\omega^{2\gamma}\sin^2\frac{\pi\gamma}{2},$$
$$s = \frac{M\omega^{1+\gamma}\sin\frac{\pi\gamma}{2}}{r},$$
$$v = \omega\left(1 + M\omega^\gamma\cos\frac{\pi\gamma}{2}\right), \quad u = \frac{v}{r},$$
$$n = M\omega^{1+\gamma}\sin\frac{\pi\gamma}{2} - \frac{\omega^2}{2},$$
$$g = -p(1-\hat{e}^{-s}\cos u) - q\hat{e}^{-s}\sin u + v,$$
$$h = -q(1-\hat{e}^{-s}\cos u) + p\hat{e}^{-s}\sin u - n.$$

We interpret this dispersion as an intrinsic property of the material that is overlain with the response of the charge carriers present due to doping. The explicit expression for the dispersive DOS model thus reads

$$\varepsilon'_{\mathrm{DOS},d} = \frac{qd^2N}{2\varepsilon_0 U_{\mathrm{bi}}}\left(1 - \mathrm{erf}\left[\frac{k_B T}{\sqrt{2}\sigma}\ln\frac{f}{f_0}\right]\right) + \frac{\varepsilon_{\infty,d}}{2}\frac{\omega^2 h}{g^2+h^2}. \quad (9)$$

III. EXPERIMENTAL

A. Sample preparation

We use the well-studied system of P3HT:PCBM to test the compatibility of our formalism with actual measurement data. In order to enable a fast doping process, a top electrode open to the diffusion of oxygen into the active layer was chosen. To this end we decided for an inverted architecture that allows the placement of a conductive hole injection layer on top of the photoactive material.

After thoroughly cleaning the glass/ITO substrates (15Ω/□) by sonication in acetone and isopropanol, a hole-blocking layer was applied. As a next step, the P3HT:PCBM (ratio 1:0.8 w/w; 250 nm) photoactive layer was cast, followed by a highly conductive PEDOT:PSS formulation (H. C. Starck, 50 S/cm; 200–300 nm), which acts as both, hole transport layer and electrode. All layers are applied by doctor blading from solution. The devices were completed by thermally evaporating a 500-nm-thick silver grid, consisting of fingers of 0.15 mm in width at distances of 2 mm.

Before depositing the metal grid, all cells were annealed in nitrogen at 140 °C for 5 min. The processing of the cells is described in more detail in Ref. 7.

Prior to measurement, the samples were illuminated for 1 h with a halogen lamp (approximately 2.5 suns) in synthetic air. Illuminating the samples speeds up the process of doping dramatically. The mechanism of oxygen doping of P3HT is described in detail in Refs. 7 and 22.

B. Sample chamber

The sample was placed inside a custom-made sample chamber for measurement. The actual probe stage can be actively heated as well as cooled. A Pt100 resistance thermometer is attached to the probe stage that allows a Linkam TP 93 temperature controller to maintain a constant stage temperature. All measurements are done at 25 °C. The atmosphere in the sample chamber can be changed from dry nitrogen to dry synthetic air (80% N_2, 20% O_2). Illumination is done with a halogen lamp through a glass window.

C. Electrical characterization

The dielectric measurements were performed using a Hewlett-Packard 4284A LCR meter or an Agilent 4285A LCR meter with the device kept in the dark. Both instruments were used in combination to cover the frequency range from 20 Hz to 10 MHz. The ac stimulus was as small as 5 mV to maintain the linearity of the current response. The LCR meters were computer controlled using a custom measurement software.

The complex permittivity $\varepsilon = \varepsilon' + \hat{\imath}\varepsilon''$ is obtained from the measured complex impedance $Z = Z' + \hat{\imath}Z''$. To compensate for parasitic serial impedances, the sample was connected using the four terminal pair (4TP) configuration. This measurement is performed with two independent electrical circuits; hence, every electrode is equipped with two adjacent contact points. Via the first circuit, the voltage is applied and the resulting current through the sample is measured, while the second measures the voltage drop across the sample. This configuration reduces the parasitic serial impedance to approximately 2.5Ω, for which the measured impedance is corrected. Moreover, the current-voltage (IU) characterization was performed with a Keithley 2400 Source Meter in 4TP mode. The 4TP configuration is described in detail in Ref. 23.

IV. RESULTS AND DISCUSSION

The black circles in Fig. 2 show the real part of the measured relative permittivity. At low frequencies (20 Hz to 100 kHz) a plateau with a relative permittivity between 25 and 30 is visible. A transition in the dielectric response toward lower values is observed between 100 kHz and 1 MHz, which is almost symmetric in logarithmic frequency space. This transition is followed by the high-frequency plateau with a relative permittivity around 3.

The static DOS model [Eq. (8)], the dispersive DOS model [Eq. (9)], and the Debye relaxation model [Eq. (1)] were fitted

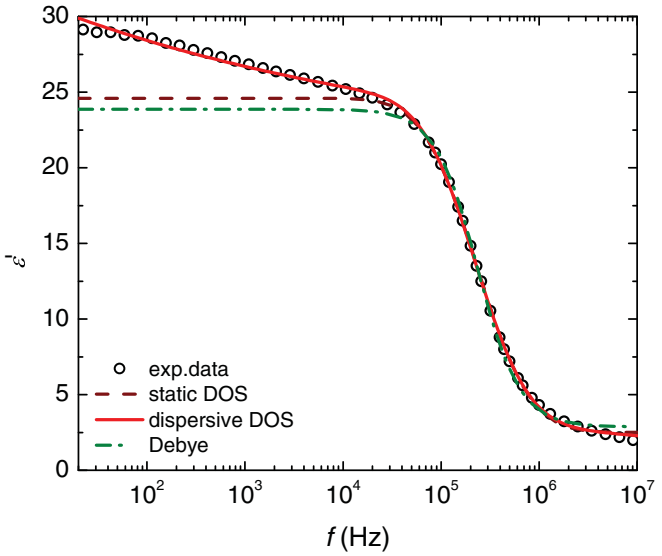

FIG. 2. (Color online) Real part of the relative permittivity of a doped P3HT:PCBM-based device (black circles). The lines represent best fits to the data using the formalism of the static and the dispersive DOS models as well as Debye relaxation.

to the experimental data. The fits are shown as lines in Fig. 2. The static DOS model and the Debye relaxation model were fitted between 20 kHz and 10 MHz, whereas the dispersive DOS model was fitted to the whole measurement range from 20 Hz to 10 MHz. The constraints in the frequency range are necessary since only the dispersive DOS model can account for the slope of ε' observed at low frequencies. Tables I to III list the parameters obtained from fitting the respective model to the experimental data.

All three formalisms allow to reproduce the experimentally observed transition between the two capacitance regimes at around 230 kHz. The characteristic frequency corresponding to τ obtained from fitting the real part of the Debye relaxation model [Eq. (1)] to the experimental data is given by $(2\pi\tau)^{-1}$. We relate the inverse of the characteristic frequency to the average time a charge carrier needs to travel from one electrode to the other. This time is dominated by the period the charge carrier spends inside traps as demonstrated by Parisi *et al.*[17]

For the DOS models, the height of the step $\Delta\varepsilon$ and the concentration of dopants N are related via $\frac{qd^2N}{\varepsilon_0 U_{\mathrm{bi}}}$. Debye relaxation directly fits the parameter $\Delta\varepsilon$ and gives no physical picture that describes the constitution of this value. Neither do the equivalent circuits. All models allow accommodation of a height of the step of about 21. Assuming a built-in voltage of approximately 1 V yields a concentration of dopants in the order of magnitude of $10^{16}\mathrm{cm}^{-3}$ for the given surface area of $A = 80\ \mathrm{mm}^2$. This is consistent with values reported for

TABLE I. Parameters obtained from fitting the static DOS model [Eq. (8)] to the experimental data (see Fig. 2) in the frequency range between 20 kHz and 10 MHz.

N/U_{bi} ($\mathrm{cm}^{-3}\mathrm{V}^{-1}$)	f_0 (kHz)	σ (meV)	$\varepsilon_{g,s}$ (1)
3.05×10^{16}	230	23	2.51

TABLE II. Parameters obtained from fitting the dispersive DOS model [Eq. (9)] to the experimental data (see Fig. 2) in the frequency range between 20 Hz and 10 MHz.

N/U_{bi} ($\mathrm{cm}^{-3}\mathrm{V}^{-1}$)	f_0 (kHz)	σ (meV)	$\varepsilon_{\infty,d}$ (1)	M (1)	γ (1)
2.84×10^{16}	224	22	0.0021	2562	0.89

TABLE III. Parameters obtained from fitting the Debye relaxation model [Eq. (1)] to the experimental data (see Fig. 2) in the frequency range between 20 kHz and 10 MHz.

$\Delta\varepsilon$ (1)	ε_∞ (1)	τ (*ns*)
21	2.87	675

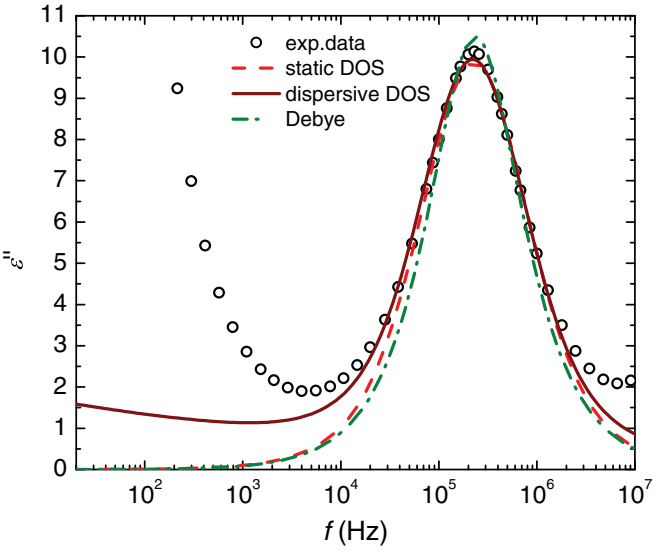

FIG. 3. (Color online) Imaginary part of the relative permittivity of a doped P3HT:PCBM-based device (black circles). The lines are derived from parameters obtained by fitting the respective model to the real part of the relative permittivity.

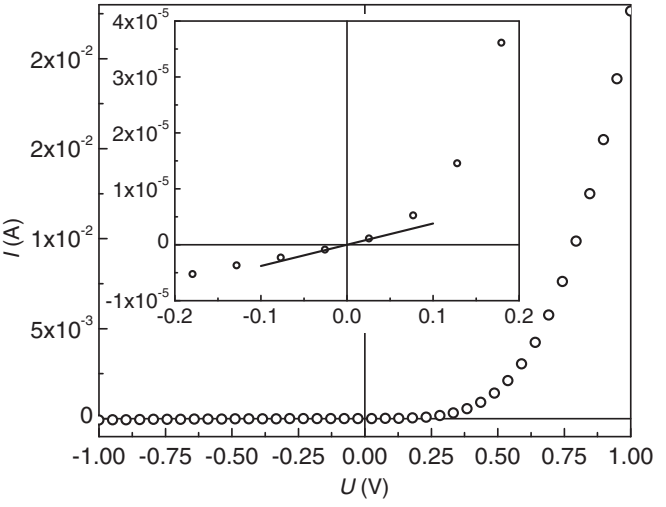

FIG. 4. Current-voltage curve. (Inset) A detailed view of the region around 0V. The solid line is a fit of Ohm's law to the two data points measured at ±25 mV.

P3HT:PCBM by applying Mott-Schottky analysis or charge extraction by linearly increasing voltage (CELIV).[7,10] The dispersive DOS model yields a concentration of dopants that is smaller by about 7% because the dispersivity of the geometric permittivity also contributes to the height of the step which in the static DOS model is entirely assigned to the concentration of dopants. Figure 3 shows the experimental data on the imaginary part of the relative permittivity as black circles. The main feature is a peak between 100 kHz and 1 MHz. Toward low frequencies ε'' increases with $1/f$.

The lines in Fig. 3 do not represent best fits to the data but are derived from the parameters given in Tables I to III. The graphs for the static and the dispersive DOS model were obtained from the numeric Kramers-Kronig transformation [Eq. (7)] of the real part. The curve representing the Debye relaxation formalism is based on Eq. (2) and the parameters listed in Table III.

The peak between 100 kHz and 1 MHz that is caused by relaxation is described very well by both models. The increase with $1/f$ of ε'' at low frequencies is associated with the contribution of the finite dc resistance to the dielectric response. This resistance is estimated from the slope of the dark IU curve around $0V$ as illustrated in Fig. 4. Its inset depicts a detailed view of the region around $0V$. The solid line in the inset is a fit of Ohm's law to the two data points measured at $[\pm 25]mV$, yielding a resistivity of $R = 26.2\ \mathrm{k}\Omega$.

Equation (3) allows incorporation of the contribution of the finite dc resistance into the imaginary part of the relative permittivity. Taking this into account yields the corrected ε'' derived from the fit formalisms to ε' shown in Fig. 5. As stated by Eq. (3), a frequency-independent resistor causes a contribution that is proportional to $1/\omega$ as illustrated by the orange line in the inset of Fig. 5 (note the double-logarithmic scaling). This correction results in an excellent agreement between the experimental data and the theoretical curves in the low-frequency regime.

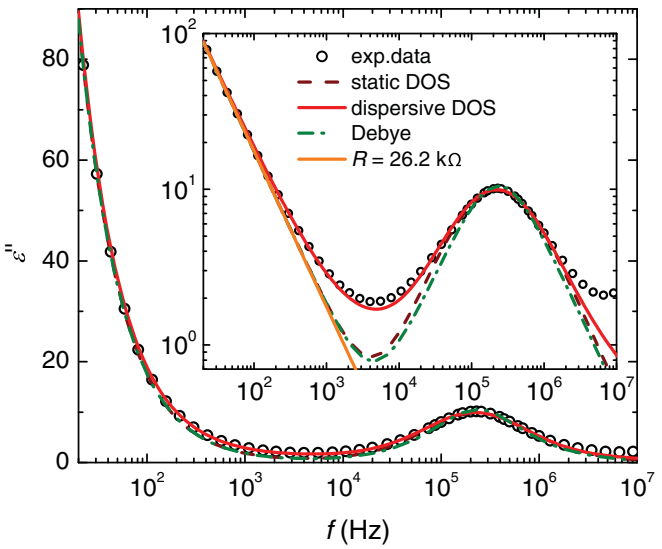

FIG. 5. (Color online) Imaginary part of the relative permittivity (black circles). The lines are derived using parameters obtained from fitting the respective model to the real part of the relative permittivity and an additive contribution from a frequency-independent parallel resistance of $R = 26.2\ \mathrm{k}\Omega$.

V. CONCLUSION

We presented a model describing the frequency response of the dielectric permittivity of doped organic semiconductor devices. The formalism was applied to experimental data measured on oxygen-doped, state-of-the-art P3HT:PCBM-based organic solar cells. Doping processes introduce additional charges that are assumed to get trapped and to contribute to the capacitance upon re-emission. Together with the assumption of a frequency-dependent geometric capacitance introduced by Martens *et al.*, excellent agreement with the measured real part of the dielectric function is obtained. We compared our formalism to well-established alternative approaches such as two commonly used equivalent circuits as well as standard Debye relaxation. Not only does the dispersive DOS model exhibit a superior fit to the experimental device data over the studied frequency range of five orders of magnitude, it also gives direct insight into the concentration of charge carriers introduced by doping. We determine a concentration of dopants in the order of magnitude of $10^{16}\ \mathrm{cm}^{-3}$, which is in excellent agreement with results of other methods such as Mott-Schottky analysis or CELIV. One of the advantages over the latter two techniques is that no dc bias needs to be applied, which induces unwanted current through the device as the conductivity increases with ongoing doping, an undesired effect complicating the analysis.[7] Our approach hence enables impedance spectroscopy to be used as a convenient tool to determine the extrinsic charge carrier concentration in functional organic electronics devices. As these charges are induced from, e.g., exposure to oxygen and deteriorate the device performance, this offers a route to better study this important degradation mechanism.

In order to fit the imaginary part of the dielectric function, we performed a Kramers-Kronig transformation of our formalism. For good agreement with the experimental data, a correction for the parallel resistance of the device obtained from the slope of the current-voltage characteristic around 0 V is necessary. The low-frequency regime is dominated by the contribution of this resistance, whereas the high-frequency peak is accounted for by the influence of the extrinsic charge carriers. We consider the excellent agreement between experimental data and the Kramers-Kronig transform of our dispersive DOS model as a support of our approach in which we favored a direct link between a physical process and the experimental observation over a detour via equivalent circuits or Debye relaxation.

ACKNOWLEDGMENTS

The authors are indebted to Professor Eitan Ehrenfreund for his explicit derivation of ε' from the complex admittance representation chosen by Martens *et al*. Financial support by the German Ministry for Education and Research (BMBF) is acknowledged (projects "OPV Stability," FKZ 03SF0334A, and "EOS," FKZ 03X3516B).

*Present address: Department of Physical Chemistry, University of Vienna, Währinger Straße 42, A-1090 Vienna, Austria; oskar.armbruster@univie.ac.at

†Present address: Konarka Technologies, Inc., 116 John Street, Lowell, MA 01852, USA; clungenschmied@konarka.com

[1] *BP Statistical Review of World Energy* (June 2010).

[2] A. Jäger-Waldau, PV Status Report 2010 (JRC Scientific and Technical Reports, Ispra, 2010).

[3] M. A. Green, K. Emery, Y. Hishikawa, and W. Warta, Prog. Photovolt: Res. Appl. **19**, 84 (2010).

[4] M. A. Green, K. Emery, Y. Hishikawa, and W. Warta, Prog. Photovolt: Res. Appl. **18**, 346 (2010).

[5] C. J. Brabec, S. Gowrisanker, J. J. M. Halls, D. Laird, S. Jia, and S. P. Williams, Adv. Mater. **22**, 3839 (2010).

[6] M. Jørgensen, K. Norrman, and F. C. Krebs, Sol. Energy Mater. Sol. Cells **92**, 686 (2008).

[7] A. Seemann, T. Sauermann, C. Lungenschmied, O. Armbruster, S. Bauer, H.-J. Egelhaaf, and J. Hauch, Solar Energy **85**, 1238 (2011).

[8] H. C. F. Martens, H. B. Brom, and P. W. M. Blom, Phys. Rev. B **60**, 8489 (1999).

[9] J. Scherbel, P. H. Nguyen, G. Paasch, W. Brütting, and M. Schwoerer, J. Appl. Phys. **83**, 5045 (1998).

[10] P. P. Boix, G. Garcia-Belmonte, U. Muñecas, M. Neophytou, C. Waldauf, and R. Pacios, Appl. Phys. Lett. **95**, 233302 (2009).

[11] F. Kremer and A. Schönhals, eds., *Broadband Dielectric Spectroscopy* (Springer-Verlag, Berlin, 2003).

[12] S. Nowy, W. Ren, A. Elschner, W. Lövenich, and W. Brütting, J. Appl. Phys. **107**, 054501 (2010).

[13] J. D. Cohen, Semicond. Semimet. **21**, 9 (1984).

[14] S. S. Hegedus and E. A. Fagen, J. Appl. Phys. **71**, 5941 (1992).

[15] T. Walter, R. Herberholz, C. Müller, and H.-W. Schock, J. Appl. Phys. **80**, 4411 (1996).

[16] R. Schmechel, Phys. Rev. B **66**, 235206 (2002).

[17] J. Parisi, V. Dyakonov, M. Pientka, I. Riedel, C. Deibel, C. J. Brabec, N. S. Sariciftci, and J. C. Hummelen, Z. Naturforsch. A **57a**, 995 (2002).

[18] H. Bässler, Phys. Status Solidi B **107**, 9 (1981).

[19] H. Bässler, Phys. Status Solidi B **175**, 15 (1993).

[20] R. de Laer Kronig, J. Opt. Soc. Am. **12**, 547 (1926).

[21] J. D. Jackson, *Classical Electrodynamics*, 3rd ed. (John Wiley & Sons, Inc., New York, 1999).

[22] G. Dennler, C. Lungenschmied, N. S. Sariciftci, R. Schwödiauer, S. Bauer, and H. Reiss, Appl. Phys. Lett. **87**, 163501 (2005).

[23] *Agilent Impedance Measurement Handbook*, Agilent Technologies, Inc., 4th ed. (2009).